OPTIMAL TAKEOFF AND LANDING OF HELICOPTERS FOR ONE-ENGINE-INOPERATIVE OPERATION

BY

YOSHINORI OKUNO AND KEIJI KAWACHI

UNIVERSITY OF TOKYO

4-6-1 KOMABA MEGUROKU TOKYO 153, JAPAN

SHIGERU SAITO

NATIONAL AEROSPACE LABORATORY, TOKYO, JAPAN

AND

AKIRA AZUMA

TOKYO METROPOLITAN INSTITUTE OF TECHNOLOGY, TOKYO, JAPAN

FIFTEENTH EUROPEAN ROTORCRAFT FORUM

SEPTEMBER 12 - 15, 1989   AMSTERDAM

Optimal Takeoff and Landing of Helicopters
for One-Engine-Inoperative Operation

Yoshinori Okuno* and Keiji Kawachi†
University of Tokyo, Tokyo, Japan

Shigeru Saito§
National Aerospace Laboratory, Tokyo, Japan
and
Akira Azuma‡
Tokyo Metropolitan Institute of Technology, Tokyo, Japan

Nonlinear optimal control theory is applied to the takeoff and landing of helicopters in case of an engine failure. Four types of the optimization problems are formulated: (i) minimization of the touchdown speed, (ii) minimization of the height loss during OEI transition, (iii) minimization of the restricted region in the H-V diagram, and (iv) maximization of the takeoff weight for Category A VTOL operation. Predictions of the H-V diagrams and the operating limitations for Category A show good correlations with the flight test results for several helicopters over a wide range of the operating conditions. Some non-optimal controls conducted by the pilots during the tests are also discussed.

1. Introduction

A helicopter – whether single or twin engined – has a chance to make a safe landing following an engine failure except for some initial conditions of the height and velocity. If these conditions are sufficient to the transition into forward flight on the remaining power, a twin engine helicopter has another chance to fly away. Such information, usually illustrated as height-velocity (H-V) diagrams, has the greatest importance for the planning of Category A operation. The typical takeoff paths for Category A are schematically shown in Fig.1. If an engine failure occurs before reaching the critical decision point (CDP), the helicopter must be landed immediately. The speed at the CDP is restricted by the distance of this rejected takeoff.

The smaller the heliport size, the lower the allowable CDP speed. Once past the CDP, the takeoff must be completed with a clearance of at least 35 ft from the ground. This condition determines the height of the CDP. The lower the CDP speed, the higher the CDP height. If the CDP is located in or above the restricted region in the H-V diagram, the payload must be reduced. Consequently, the performance for one engine inoperative (OEI) operations is closely connected with the economics of the helicopter operation.
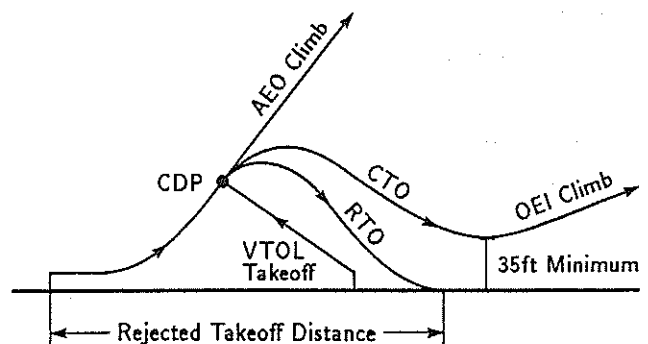

Fig.1 Category A Takeoff Profile.

---

* Graduate Student, Department of Aeronautics.
† Associate Professor, Research Center for Advanced Science and Technology.
§ Senior Researcher.
‡ Professor.

Flight tests are usually conducted to verify the safety in case of an engine failure. They, however, require much cost and time because of the high risk. In order to support these tests, simulation models have been highly developed in recent years (Refs.[1-4]). Nevertheless, only simple point-mass models have been used in the applications of the optimal control theory, which reduced the reality of the solutions (Refs.[5-7]). In Ref.[8], the authors applied nonlinear optimal control theory to the rigid body dynamic performance model combined with the experimentally verified aerodynamic model. In this paper, this method is extended to predict the H-V diagram and the maximum performance for Category A operation.

2. Formulation of the Optimization Problems

2.1 Equations of Motion

In this paper, a rigid body model with three degrees of freedom is used to evaluate the dynamic performance of the helicopter. The state variables are height loss, horizontal and vertical velocities, pitch attitude, pitch rate, and rotational speed of the main rotor. The control variables are collective pitch and longitudinal cyclic pitch. The equations of motion are given in Appendix A-1. The external forces taken into account are thrust, H-force, torque, and longitudinal hub moment of the main rotor, drag of the body, lift of the horizontal stabilizer, etc. The aerodynamic performance of the main rotor is calculated based on the modified momentum theory and the modified blade element theory. This model is applicable to the vortex ring state and considers the effect of the blade stall during descending flight. The details of this model are contained in Ref.[8]. The equations of the aerodynamic coefficients of the main rotor are given in Appendix A-2. The flapping motion is assumed to be quasi-steady. A hingeless rotor is substituted by an articulated rotor with the equivalent hinge offset. The flapping equations[9] are given in Appendix A-3.

2.2 Performance Index and Boundary Conditions

Four types of the optimization problems in case of an engine failure are formulated as follows:

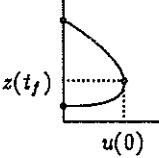(i) Minimization of the touchdown speed for a given set of the initial flight conditions.

(ii) Minimization of the height loss during the transition into the level flight on the remaining power.

(iii) Minimization of the restricted region in the H-V diagram. In this paper, an H-V diagram is estimated by calculating three key points: high hover point, knee point, and low hover point. The definitions of 'minimization of the restricted region' for each point are as follows: (iiia) For the high hover point, minimization of the initial hovering height under the conditions that the horizontal and vertical touchdown speeds are within the respective capabilities of the landing gear. (iiib) For the knee point, minimization of the initial velocity. The height of the knee point is determined to maximize the minimum initial velocity. (iiic) For the low hover point, maximization of the initial height.

(iv) Maximization of the takeoff weight for Category A VTOL operation. The most critical height for a rejected takeoff is approximately the height of the knee point in the H-V diagram, which is usually lower than the CDP height of the VTOL takeoff procedure. It is required, therefore, to eliminate the restricted region in the H-V diagram. Thus, this problem is equivalent to the maximization of the weight under the condition that the helicopter can be landed within the allowable touchdown speed from any initial height if an engine failure occurs in hover.

The performance indices and the boundary conditions for these four (six) problems are given in Table.1.

Table.1 Performance Indices and Boundary Conditions.

Problem		Performance Index	Initial Conditions	Terminal Conditions
Min. Touchdown Speed		$\min \sqrt{\left(\frac{u(t_f)}{u_s}\right)^2 + \left(\frac{w(t_f)}{w_s}\right)^2}$	$u(0), w(0), \Omega(0)$; given $\Theta(0)$; given from trim conditions $z(0), q(0) = 0$	$z(t_f)$; given, $\Theta(t_f), q(t_f)$; given or free
Min. Height Loss during CTO		$\min z(t_f)$		$w(t_f) = 0, u(t_f)$; given, $q(t_f) = 0, \Theta(t_f)$; free
H-V Diagram	Min. Height of High Hover Point	$\min z(t_f)$		$\sqrt{\left(\frac{u(t_f)}{u_s}\right)^2 + \left(\frac{w(t_f)}{w_s}\right)^2} = 1,$ $\Theta(t_f), q(t_f)$; given or free, $z(t_f)$; free
	Min. Speed of Knee Point	$\max\limits_{z(t_f)} \min u(0)$	$u(0)$; free	
	Max. Height of Low Hover Point	$\max z(t_f)$		
Max. Weight for Category A VTOL Operation (for Elimination of Restricted Region)		$\min\limits_{z(t_f)} \max m$	$u(0) = 0$	

2.3 Constraints

In this paper, the following constraints are considered: (1) and (2) range of the control variables, (3) maximum value of the averaged resultant angle of attack of the blade at $0.75R$, (4) maximum value of the vertical load factor, (5) range of the pitch attitude, and (6) range of the rotor speed. They are expressed as

$$\theta_{0min} \le \theta_0 \le \theta_{0max} \tag{1}$$

$$\theta_{smin} \le \theta_s \le \theta_{smax} \tag{2}$$

$$\alpha_r \equiv \theta_0 - \frac{4}{3}\lambda \le \alpha_{max} \tag{3}$$

$$\frac{dw}{dt} \ge g\left(1 - n_{max}\right) \tag{4}$$

$$\Theta_{min} \le \Theta \le \Theta_{max} \tag{5}$$

$$\Omega_{min} \le \Omega \le \Omega_{max} \tag{6}$$

Only for the cases of fly-away (problem (ii)), two more constraints are imposed to obtain realistic solutions. They are

$$w \ge w(0)\{1 + \cos(\pi t/t_f)\}/2 \tag{7}$$

$$\frac{du}{dt} \ge 0 \tag{8}$$

These inequality constraints are transformed into equality constraints by introducing 'slack variables'[10].

These nonlinear optimal control problems are numerically solved through the use of Sequential Conjugate Gradient Restoration Algorithm[11].

3. Prediction of H-V Diagram

3.1 H-V Diagrams of Single Engine Helicopters

Fig.2 shows the H-V diagrams of two single engine helicopters (S-58 and Hughes 269, refer to Table.A-1). The predictions by the present theory correlate well with the flight test data[12,13] especially in the vicinity of the knee points. The velocities and the heights of the knee points are different between two helicopters, though the heights of the high hover points are almost the same. This is mainly caused by the different capacities of the landing gears.

Fig.3 shows the control histories of the above exemplified helicopters for the cases of landing from the high hover points. It is observed that the pitching motions of both helicopters are similar to the optimal solutions. The pilot of the S-58 helicopter, however, conducted the collective flare
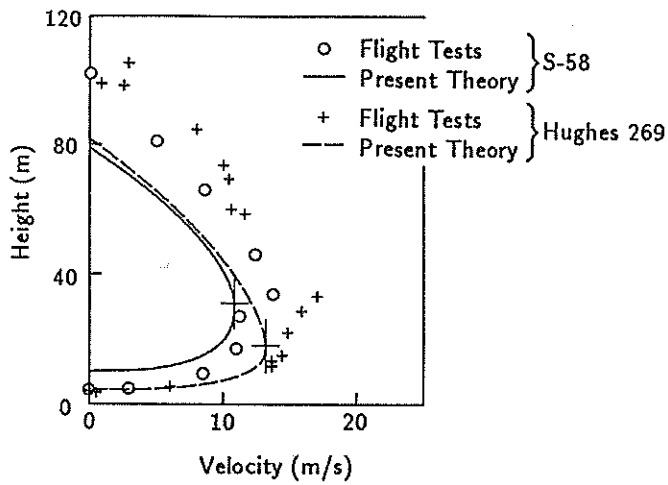
Fig.2 H-V Diagram Predictions of the Single Engine Helicopters.

earlier than the optimal timing. This might be due to the steep and high rate descent. On the other hand, the amplitude of the collective flare conducted by the pilot of the Hughes 269 is lower than the optimal solution. This follows that the kinetic energy of the rotor remained unused at the time of touchdown as observed in the time history of the rotor speed. Not only the theoretical errors but these non-optimal controls by the test pilots cause the discrepancies between the theoretically predicted and the experimentally determined H-V diagrams.
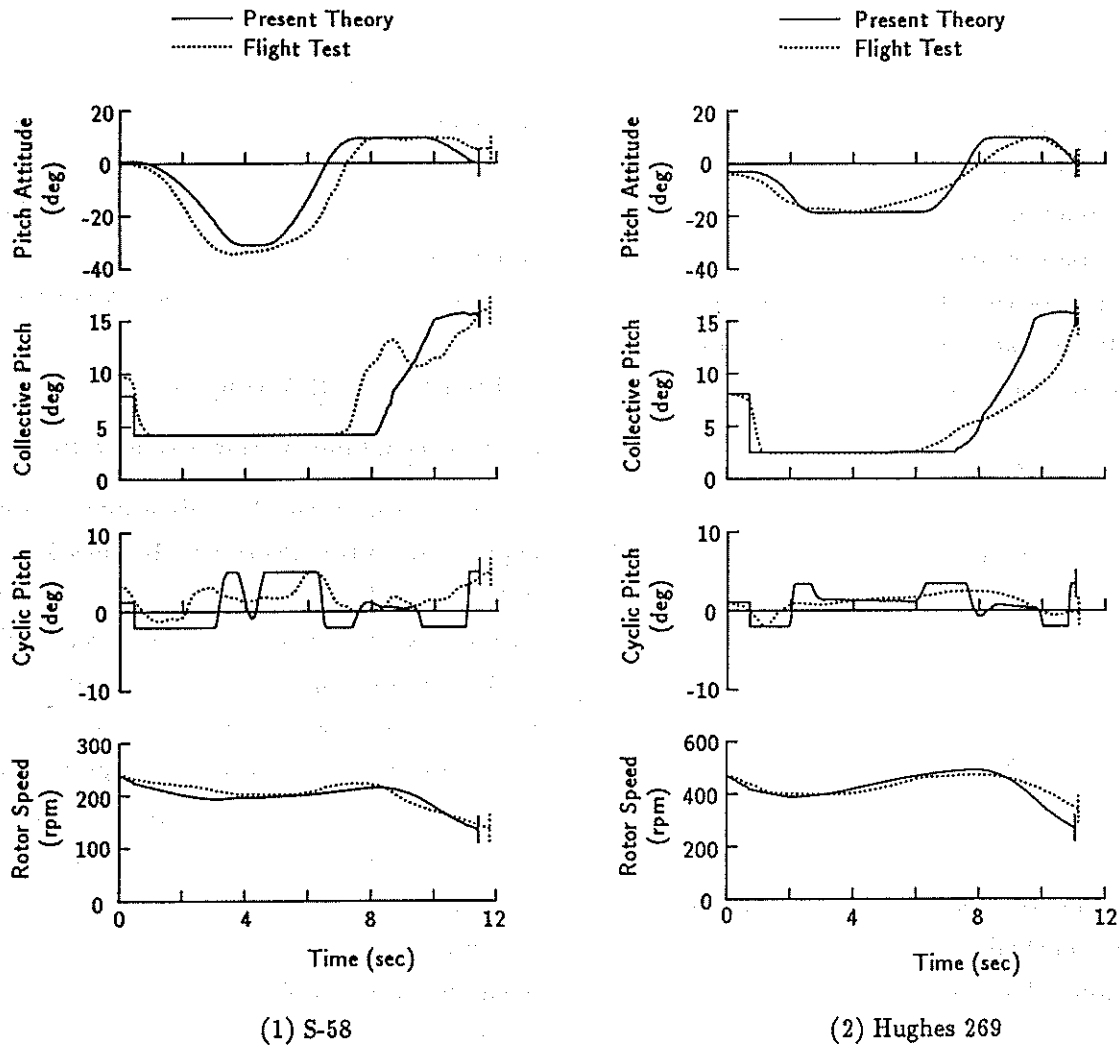

(1) S-58

(2) Hughes 269

Fig.3 Control Histories for the Single Engine
Helicopters Landing from High Hover Point.

In order to make clear the effects of the differences in the dynamic and aerodynamic models on the prediction of an H-V diagram, comparisons are made between four combinations of these models as shown in Fig.4. The point-mass dynamic model predicts unreasonable restricted regions, though it has an advantage of simplicity of the formulation. The simple aerodynamic model, which neglects the influence of stall at the blade root and the increased induced power in the vortex ring state, reduces the accuracy of the prediction.

3.2 H-V Diagrams of Twin Engine Helicopters

Fig.5 shows the H-V diagram of a twin engine helicopter (YUH-61A). The present theory predicts the boundary of the fly away possible region in good accordance with the flight test results[14] except for the cases of low initial speed. The control histories for this case of fly away from hovering are shown in Fig.6. The differences between the optimal solution and the flight test data are remarkable in the histories of rate of descent. The test pilot conducted a nose-up maneuver and reduced
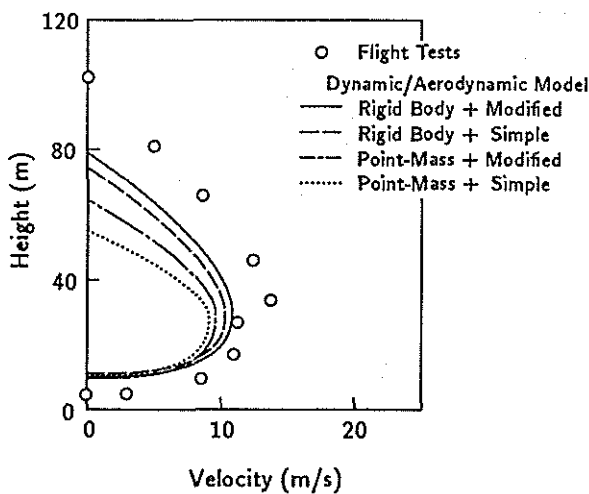

Fig.4 Effects of the Dynamic and Aerodynamic Models on H-V Diagram Prediction.
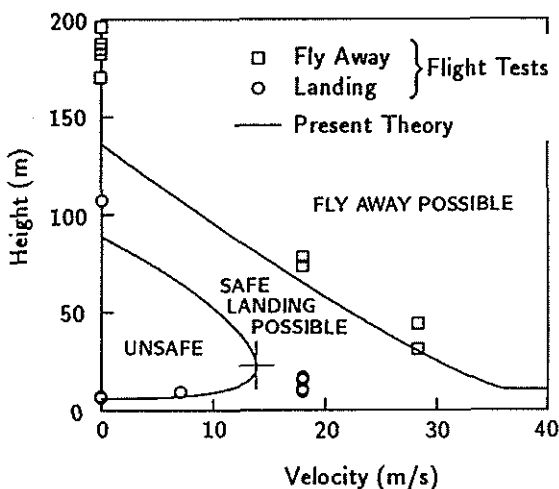
Fig.5 H-V Diagram Prediction of the Twin Engine Helicopter.
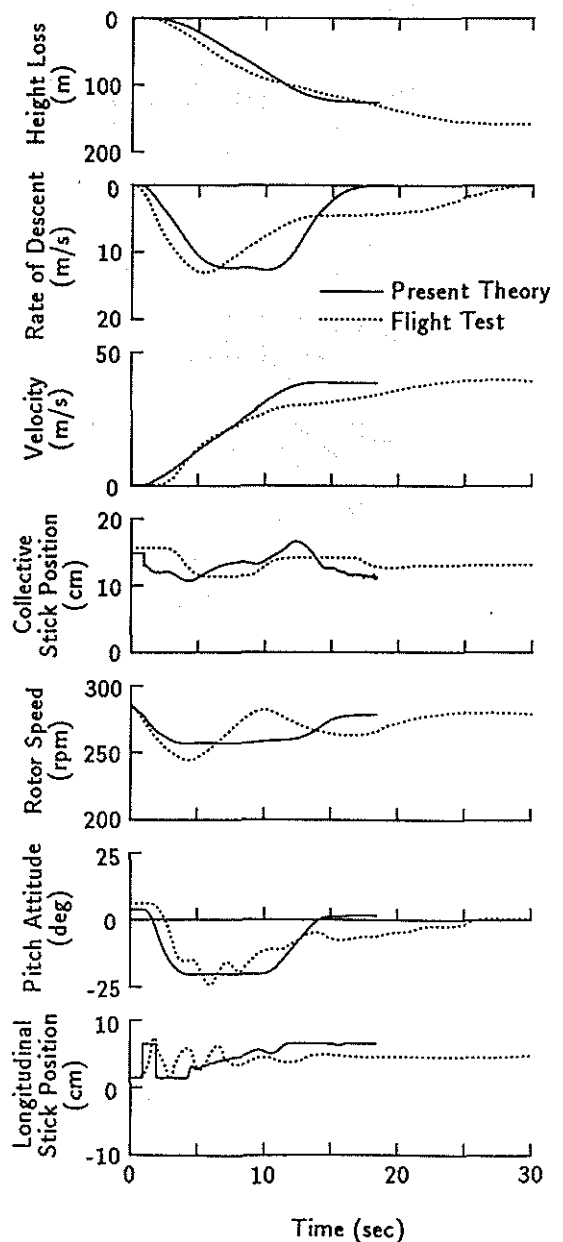
Fig.6 Control Histories for the Case of Fly-Away.

the sinking rate earlier than the optimal timing. This resulted in the insufficient forward speed and the long duration of the slight descent.

The size of the restricted region in the H-V diagram depends on the various operating conditions. The effects of the outside air temperature, the pressure altitude, and the gross weight on the height of the high hover point of a twin engine helicopter (BK117) are shown in Fig.7. The correlations between the predictions and the certification data are close especially for the extreme conditions such as high altitude and high temperature. This trend is related to the available power of the residual engine as mentioned below. Fig.8 shows the control histories for the case of landing from the high hover point under a moderate ambient condition. It is observed from the flight test data that
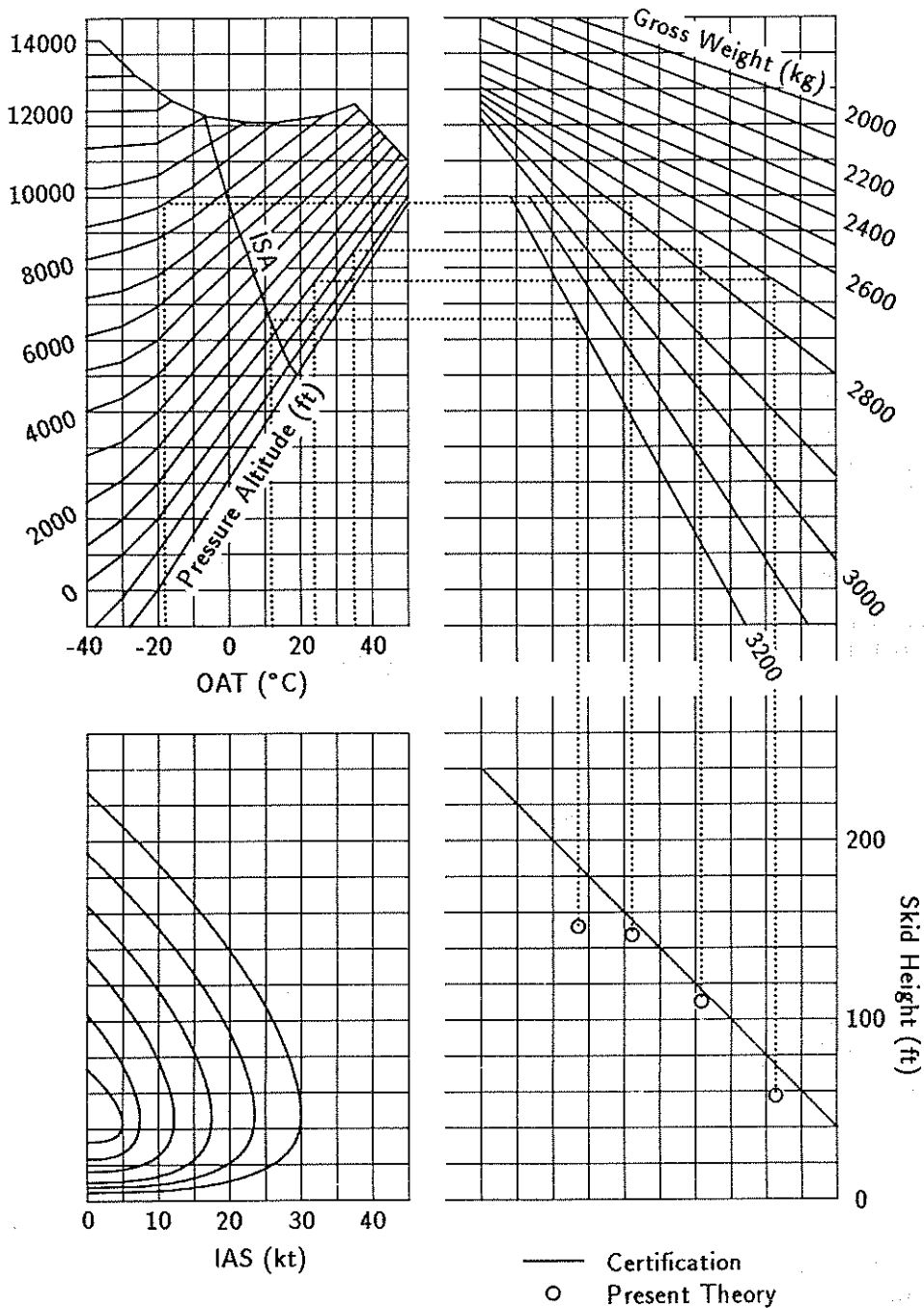
Fig.7 Effects of the Operating Conditions on H-V Diagram Prediction.

the engine torque is reduced to prevent the rotor from overspeed. In this paper, the available engine torque variation with the rotor speed is assumed as shown in Fig.9. The maximum torque is derived from the engine power chart as a function of the pressure altitude and the air temperature. The optimal solution indicates that the rotor speed should be kept so that the full engine torque is available. Under the extreme conditions, the available power is not enough to keep the high rotor speed and does not cause this difference between the flight test data and the optimal solution.

Another noticeable difference is sought in the time histories of collective pitch in Fig.8. The test pilot did not distinctly conduct collective flare in contrast to the optimal solution. This type of the collective pitch control without the flare appears in the optimal solutions only when the initial height is relatively low as exemplified in Fig.10. Under such conditions, there is no time before landing to exchange the height loss for the kinetic energy and to store it as a rotor rotational energy.

Fig.8 Control Histories for the Twin Engine Helicopter Landing from High Hover Point.

Fig.9 Estimated Engine Torque Variation with Rotor Speed.

Fig.10 Effect of the Initial Hovering Height on the Optimal Histories of Rotor Speed.

4. Prediction of Category A Takeoff Performance

When there is no restriction on the available heliport size, the maximum weight for Category A (STOL) operation is usually determined by the capability of climbing at least 100 fpm in case of an engine 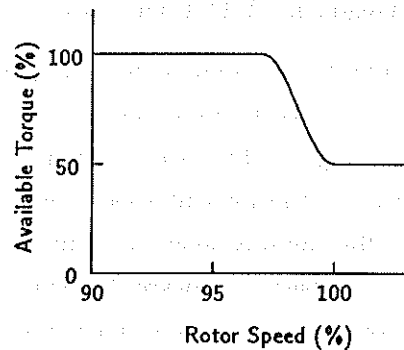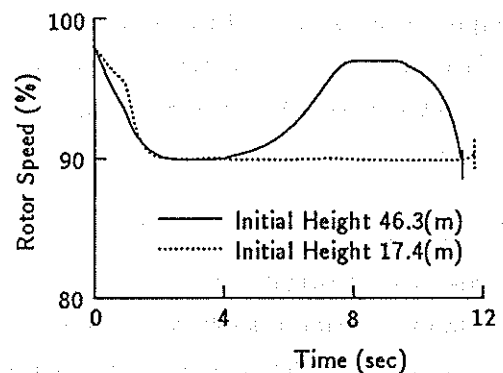failure. Consequently, there is no interest as an optimal control problem in maximizing the weight limitation. For Category A VTOL operation from a small heliport, however, the maximum weight is limited by the safe landing capability in case of a rejected takeoff. Discussed in the following sections are the maximum weight for Category A VTOL operation and the allowable takeoff trajectories for Category A STOL operation.

4.1 Maximum Weight for VTOL Operation

The maximum takeoff weights for Category A VTOL operation of a twin engine helicopter (BK 117) are shown in Fig.11. The circular symbols indicate the results by the present theory with the 30% margin of the landing gear capabilities (20 kt forward and 8 ft/sec downward for this helicopter). These results are in accordance with the data for certification better than the results with 100% touchdown speed. This is because the certification source might be more conservative than the maximum performance. Another reason is that this is the case for VTOL operation and a very small heliport such as a roof-top is assumed, so that the forward speed at the time of touchdown might be limited lower than the maximum capability of the landing gear.

4.2 Takeoff Trajectory for STOL Operation

In order to investigate the safety in case of an engine failure during takeoff, the H-V diagram shown in Fig.12 is predicted under the condition of climbing at the flight path angle of 10°. When such an H-V diagram is available, the CDP is determined as an intersection of the takeoff trajectory and the boundary between the fly away possible region and the safe landing possible region as exemplified in Fig.12. The speed at the CDP

varies associated with the takeoff procedure from the speed of the knee point to takeoff safety speed (TOSS) at which the rate of climb of 100 fpm is enabled on the remaining power. Currently, the speed at the CDP for the usual STOL operation is selected sufficiently high as shown in Fig.12. This is based on the assumption that restrictions on the heliport size can be disregarded. The differences in the continued and the rejected takeoff trajectories between these CDP's are shown in Fig.13. A takeoff procedure with the lower speed CDP requires the shorter rejected takeoff distance.
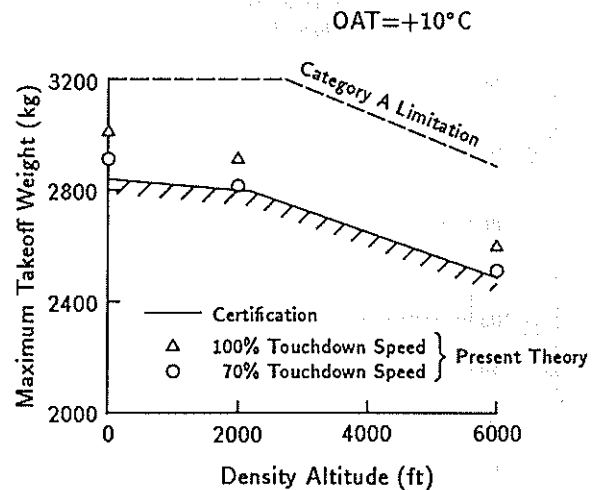

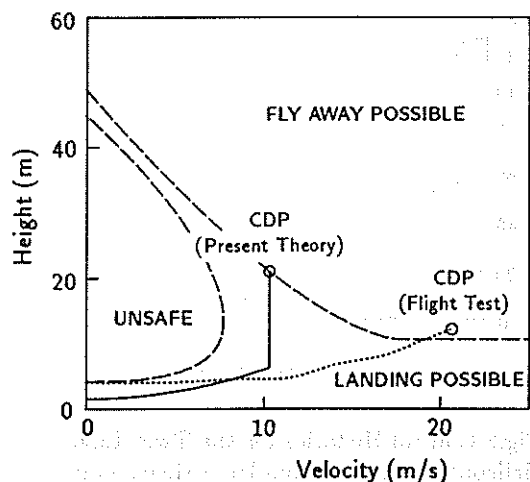Fig.11 Prediction of the Maximum Weight for Category A VTOL Operation.

Fig.12 Takeoff Trajectory and CDP in H-V Diagram.
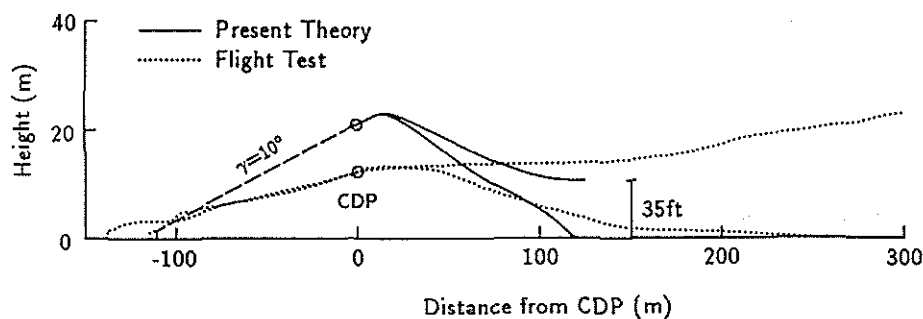
Fig.13 Continued and Rejected Takeoff Trajectories.

5. Conclusions

A numerical method to evaluate the maximum performance of helicopters under one engine inoperative conditions are presented. There is a possibility to reduce the cost, time, and risk of the flight tests and to expand the current operating limitations experimentally determined through the use of this method.

The following results are drawn in this paper:

(1) H-V diagrams of the single and the twin engine helicopters are numerically predicted in good correlation with the flight test results over a wide range of the operating conditions.

(2) Maximum weights for Category A VTOL operation of a twin engine helicopter are also predicted. Results show good agreement with the certificated maximum weights.

(3) As the speed at the CDP decreases, the rejected takeoff distance decreases though the height of the CDP increases.

(4) Some non-optimal controls conducted by the test pilots are pointed out: the premature collective flare, the insufficient collective flare, and the loss of the available power of the residual engine due to the high rotor speed.

Acknowledgments

References

[1] Cerbe, T., and Reichert, G., "Simulation Models for Optimization of Helicopter Takeoff and Landing," *Proceedings of the 13th European Rotorcraft Forum*, France, Sept. 1987.

[2] Huber, H., and Polz, G., "Helicopter Performance Evaluation for Certification," *Proceedings of the 9th European Rotorcraft Forum*, Italy, Sept. 1983.

[3] Pleasants, W. A. III, and White G. T. III, "Status of Improved Autorotative Landing Research," *Journal of the American Helicopter Society*, Vol.28, No.1, Jan. 1983, pp.16-23.

[4] Harrison, J. M., "An Integrated Approach to Effective Analytical Support of Helicopter Design and Development," *Proceedings of the 6th European Rotorcraft Forum*, England, Sept. 1980.

[5] Lee, A. Y., Bryson, A. E. Jr., and Hindson, W. S., "Optimal Landing of a Helicopter in Autorotation," *Journal of Guidance, Control, and Dynamics*, Vol.11, No.1, Jan.-Feb. 1988, pp.7-12.

[6] Johnson, W., "Helicopter Optimal Descent and Landing after Power Loss," NASA TM 73244, 1977.

[7] Komoda, M.,"Prediction of Height-Velocity Boundaries for Rotorcraft by Application of Optimization Techniques," *Transactions of the Japan Society for Aeronautical and Space Sciences*, Vol.15, No.30, 1973, pp.208-228.

[8] Okuno, Y., Kawachi, K., Azuma, A., and Saito, S., "Analytical Study of Dynamic Response of Helicopter in Autorotative Flight," *Proceedings of the 14th European Rotorcraft Forum*, Italy, Sept. 1988.

[9] Azuma, A., "Dynamic Analysis of the Rigid Rotor System," *Journal of Aircraft*, Vol.4, No.3, May-June, 1967, pp.203-209.

[10] Jacobson, D. H., and Lele, M. M., "A Transformation Technique for Optimal Control Problems with a State Variable Inequality Constraint," *IEEE Transactions on Automatic Control*, Vol.AC-14, No.5, Oct. 1969, pp.457-464.

[11] Wu, A. K., and Miele, A., "Sequential Conjugate Gradient Restoration Algorithm for Optimal Control Problems with Non-Differential Constraints and General Boundary Conditions, Part 1," *Optimal Control Applications and Methods*, Vol.1, 1980, pp.69-88.

[12] Hanley, W. J., DeVore, G., and Martin, S., "An Evaluation of the Height Velocity Diagram of a Heavy Weight, High Rotor Inertia, Single Engine Helicopter," FAA-ADS-84, 1966.

[13] Hanley, W. J., and DeVore, G., "An Evaluation of the Height Velocity Diagram of a Light Weight, Low Rotor Inertia, Single Engine Helicopter," FAA-ADS-46, 1965.

[14] Benson, G., Bumstead, R., and Hutto, A. J., "Use of Helicopter Flight Simulation for Height-Velocity Test Predictions and Flight Test Risk Reduction," *Proceedings of the 34th Annual Forum of the American Helicopter Society*, May 1978.

Notation

a = lift-curve-slope of blade section

B = tip loss factor

C_H = H-force coefficient, $C_H = H/\rho S R \Omega^2$

C_Q = torque coefficient, $C_Q = Q/\rho S R^2 \Omega^2$

C_T = thrust coefficient, $C_T = T/\rho S R \Omega^2$

C_{M_Y} = hub moment coefficient, $C_{M_Y} = M_Y/\rho S R^2 \Omega^2$

C_d, C_l = drag and lift coefficients of blade section

D = drag

g = acceleration of gravity

H = rotor H-force, positive rearward

$H_B = -T \sin i_s + H \cos i_s$

h = distance above CG, see Fig.A-1

I = moment of inertia

i_s = inclination of rotor shaft, positive forward

K_β = nondimensional flapping stiffness

$k_f = k_\beta/m_\beta R^2 \Omega^2$

k_β = spring constant of flapping hinge

L = lift

ℓ = distance behind CG, see Fig.A-1

M_Y = longitudinal hub moment, positive nose up

m = mass

n = vertical load factor

Q = required torque

Q_a = available torque

q = pitch rate, positive nose up

R = rotor radius

S = rotor disk area

T = rotor thrust

$T_B = T \cos i_s + H \sin i_s$

t_f = time of touchdown from power failure

u = horizontal velocity

$u_R = u - h_R \cdot q$

u_s = limitation of forward speed at touchdown

$\bar{v}$ = reference velocity

w = descending rate

$w_R = w + \ell_R \cdot q$

w_s = limitation of descending rate at touchdown

$\bar{x} = \int_{r_\beta}^{R} r(dm_\beta/dr)dr/m_\beta R^2$

x_s = average radius of blade stall region

α = angle of attack

β_c = longitudinal flapping angle, positive nose down

γ = flight path angle, positive climbing, or Lock number, $\gamma = \rho a c R^4/I_\beta$

Θ = pitch attitude, positive nose up

θ_s = longitudinal cyclic pitch, positive nose up

θ_t = blade twist angle, positive twist up

θ_0 = collective pitch at $0.75R$

λ = inflow ratio

μ = advance ratio

ν = descent ratio

$\bar{\nu} = bm_\beta/\rho SR$

ρ = air density

σ = rotor solidity

Ω = rotor rotational speed

Subscripts

B = relative to body-fixed axes

F = fuselage

H = horizontal stabilizer

R = rotor

β = flapping hinge

Abbreviations

AEO = all engine operating

CDP = critical decision point

CTO = continued takeoff

IAS = indicated air speed

ISA = international standard atmosphere

OAT = outside air temperature

OEI = one engine inoperative

RTO = rejected takeoff

TOSS = takeoff safety speed

Appendix

A-1. Equations of Motion

$$\frac{dz}{dt} = w$$

$$\frac{du}{dt} = -\frac{1}{m}(T_B \sin\Theta + H_B \cos\Theta + D_F \cos\alpha_F)$$

$$\frac{dw}{dt} = -\frac{1}{m}(T_B \cos\Theta - H_B \sin\Theta + D_F \sin\alpha_F) + g$$

$$\frac{d\Theta}{dt} = q$$

$$\frac{dq}{dt} = \frac{1}{I_{B_Y}}(M_Y - T_B \cdot \ell_R + H_B \cdot h_R - L_H \cdot \ell_H)$$

$$\frac{d\Omega}{dt} = -\frac{1}{I_R}(Q - Q_s)$$

A-2. Aerodynamic Coefficients of Main Rotor

$$C_T = \frac{1}{2}a\sigma\left[\frac{B^3 - kx_s^3}{3}\theta_0 - \frac{B^2 - kx_s^2}{2}\lambda + \frac{B^2 - kx_s^2}{2}\mu\theta_s\right]$$

$$C_H = \frac{1}{4}\sigma\{(1 - x_s^4)C_{\ell_0} + x_s^4 C_{\ell_s}\}\mu + \frac{1}{2}a\sigma\left[\{\frac{B^2 - kx_s^2}{4}\theta_s\right.$$
$$+ \frac{B - kx_s}{2}\mu\theta_0\}\lambda + \{-\frac{B^3 - kx_s^3}{3}\theta_0 + \frac{3(B^2 - kx_s^2)}{4}\lambda$$
$$\left. - \frac{B^2 - kx_s^2}{4}\mu\theta_s + \frac{B^2 - kx_s^2}{4}\mu\beta_c\}\beta_c\right]$$

$$C_Q = \frac{1}{8}\sigma\{(1 - x_s^4)C_{\ell_0} + x_s^4 C_{\ell_s}\}$$
$$+ \frac{1}{2}a\sigma\left[\{\frac{B^3 - kx_s^3}{3}\theta_0 - \frac{B^2 - kx_s^2}{2}\lambda + \frac{B^2 - kx_s^2}{4}\mu\theta_s\}\lambda\right.$$
$$\left. + \{-\frac{B^4 - kx_s^4}{8}\theta_s - \frac{B^2 - kx_s^2}{2}\mu\lambda - \frac{B^4 - kx_s^4}{8}\beta_c\}\beta_c\right]$$

$$C_{M_Y} = -x_\beta\frac{1}{2}a\sigma\left[\frac{B^3 - kx_s^3}{6}\cdot\frac{q}{\Omega}\right] - \frac{1}{2}x_\beta\bar{x}\bar{\nu}\beta_c - \frac{1}{2}\bar{\nu}k_f\beta_c$$

where

$$k = 1 - Cl_{stall}/Cl_{max}$$

$$x_s = \frac{1}{-2\theta_t}\left[\sqrt{\left\{\alpha_s - \left(\theta_0 - \frac{3}{4}\theta_t\right)\right\}^2 + 4\theta_t\lambda} - \left\{\alpha_s - \left(\theta_0 - \frac{3}{4}\theta_t\right)\right\}\right]$$

and where

$$\mu = \{u_x\cos(\Theta - i_s - \beta_c) - w_x\sin(\Theta - i_s - \beta_c)\}/R\Omega$$
$$\nu = \{u_x\sin(\Theta - i_s - \beta_c) + w_x\cos(\Theta - i_s - \beta_c)\}/R\Omega$$
$$\lambda = -\nu + v.$$

Here

$$\frac{\nu}{\bar{v}} = \left(\frac{v}{\bar{v}}\right)^{C_1}\sin^2\alpha_R$$
$$\pm \sin\alpha_R \cdot \sqrt{\left(\frac{\bar{v}}{\bar{v}}\right)^2 - \left(\frac{v}{\bar{v}}\right)^2\left(C_2\sin^2\alpha_R + \cos^2\alpha_R\right)}$$

where

$$\bar{v} = \sqrt{C_T/2}$$
$$\alpha_R = \tan^{-1}(\nu/\mu)$$
$$C_1 = \frac{1}{2}, \quad C_2 = \left(1 + \sqrt{2}\right)^{-4}$$

For the simple aerodynamic model,

$$x_s = 0$$
$$C_1 = 1, \quad C_2 = 0$$

A-3. Flapping Equations

$$\beta_c = \frac{K_{\dot\beta}}{K_\beta^2 + K_{\dot\beta}^2}\left\{-K_1\theta_s - 2K_2\mu\theta_0 + K_3\mu\lambda + (2 + K_\beta)\cdot\frac{q}{\Omega}\right\}$$

where

$$K_\beta = \frac{k_\beta}{I_\beta\Omega^2} + \frac{x_\beta(\bar{x} - x_\beta)}{I_\beta/m_\beta R^2}$$

$$K_{\dot\beta} = \frac{\gamma}{2}\left(\frac{1}{4}B^4 - \frac{2}{3}B^3 x_\beta\right)$$

$$K_1 = \frac{\gamma}{2}\left(\frac{B^4}{4} - \frac{B^3}{3}x_\beta\right)$$

$$K_2 = \frac{\gamma}{2}\left(\frac{B^3}{3} - \frac{B^2}{2}x_\beta\right)$$

$$K_3 = \frac{\gamma}{2}\left(\frac{B^2}{2} - Bx_\beta\right)$$

Fig.A-1 Helicopter Model.

Table.A-1 Description of the Exemplified Helicopters

Type	Max Weight (kg)	Rotor Radius (m)	Number of Engine(s)
S-58	5900	8.53	1
Hughes 269	760	3.85	1
YUH-61A	8500	7.47	2
BK117	3200	5.50	2